Nonlinear Guidance of a Human Driver via an Automated Vehicle

Bence Szaksz[1,2(✉)], Gábor Orosz[3,4], and Gábor Stépán[1,5]

[1] Department of Applied Mechanics, Budapest University of Technology and Economics, Budapest 1111, Hungary
szaksz@mm.bme.hu
[2] MTA-BME Lendület "Momentum" Global Dynamics Research Group, Budapest University of Technology and Economics, Budapest 1111, Hungary
[3] Department of Mechanical Engineering, University of Michigan, Ann Arbor 48109, USA
[4] Department of Civil and Environmental Engineering, University of Michigan, Ann Arbor 48109, USA
[5] HUN-REN–BME Dynamics of Machines Research Group, Budapest University of Technology and Economics, Budapest 1111, Hungary

Abstract. This study investigates the dynamics of a human-driven vehicle (HV) following an automated vehicle (AV) when the latter performs a guidance of the former one. After performing linear stability analysis, the relevant nonlinearity in the range policy of the human driver is taken into account, and the string stability of the system is analysed for different excitation amplitudes of the reference velocity. The results show that applying small positive values for the cruise control gain is advisable, while the backward-looking gain should somewhat be increased when the nonlinear effects are relevant.

Keywords: Autonomous vehicles · human and vehicle interaction · multi-vehicle systems · nonlinear frequency response

1 Introduction

Automated vehicles (AVs) are gaining popularity, but human-driven vehicles (HVs) are expected to continue dominating traffic in the coming years. Still, the presence of AVs has the potential to significantly influence the dynamics of traffic, particularly in terms of reducing the risk of accidents and decreasing energy consumption also for the vehicles behind them [6,7,18].

If there is no vehicle ahead of the AV then it can follow a predefined reference velocity, for which a conventional cruise control is satisfactory. However, in real-world scenarios, this free road condition cannot be assured, therefore, an adaptive cruise control (ACC) is needed. Furthermore, AVs have the potential to get information from connected human-driven vehicles (CHVs), which are located further away in the traffic. In case of connected cruise control (CCC) [20,23],

H. Yabuno et al. (Eds.): IUTAM 2023, IUTAM Bookseries 43, pp. 405–416, 2025.
https://doi.org/10.1007/978-3-031-72794-8_32

the CHV is ahead, while in case of connected traffic control (CTC) [18,28], this CHV is behind the AV. Finally, the scenario, when a pair of AVs is connected through traffic, is analyzed in [10].

String stability is a key measure for traffic dynamics, which assesses how the velocity fluctuations of a vehicle affect the velocity fluctuations of the following vehicles [3,22,26]. At the linear level, this can be described by a transfer function between the reference velocity and the velocity of a selected vehicle in the traffic (practically the last vehicle in a chain) [29]. However, transfer functions are used for linear systems, while the traffic dynamics is fundamentally nonlinear. There are various approaches for the calculation of the corresponding nonlinear frequency response functions including the harmonic balance method (HBM) [4,14,16], the Volterra series approach [13,21,24], the method of multiple scales [1,15,19], and the projection of the dynamics onto spectral submanifolds [5,11].

In this paper, the simplest traffic control scenario is considered, when an AV is driving in front of an HV. A reference velocity is provided to the AV which is utilized in its cruise controller. In the meantime, the AV also senses the velocity of the HV behind, which allows the AV to perform a guidance for the human driver. While previous studies have primarily focused on the string stability of linearized systems, here, we take into account the nonlinear range policy of the human driver, and present string stability charts for the nonlinear guidance of the HV.

The paper is organized as follows. Section 2 introduces the simplified car following model together with the corresponding control. In Sect. 3, the linearized system is analysed, which is followed by the investigation of the effect of the nonlinearities in Sect. 4. The nonlinear frequency response function is calculated with the harmonic balance method, and string stability charts are presented for certain large excitation amplitudes in the plane of the control gains of the AV. Finally, Sect. 5 includes some concluding remarks.

2 Modeling

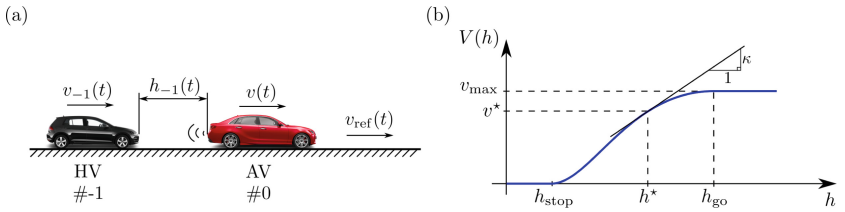

Fig. 1. Panel (a) presents the model of the guidance of a human-driven vehicle, while panel (b) shows the nonlinear range policy of the human driver.

Let us consider the simple car-following scenario when an AV is driving in front of an HV; the distance headway between the two vehicles is $h_{-1}(t)$, while the

velocities of the AV and the HV are denoted by $v(t)$ and $v_{-1}(t)$, respectively (see Fig. 1(a)). A possibly time-varying reference velocity $v_{\mathrm{ref}}(t)$ is provided to the AV that also senses the velocity difference between the two vehicles. Utilizing the translational symmetry of the system, the dynamics can be described by three first order differential equations:

$$\dot{h}_{-1} = v - v_{-1}, \tag{1}$$

$$\dot{v}_{-1} = \alpha(V(h_{-1}) - v_{-1}) + \beta(W(v) - v_{-1}), \tag{2}$$

$$\dot{v} = \hat{\beta}(v_{\mathrm{ref}} - v) + \beta_{-1}(W(v_{-1}) - v). \tag{3}$$

Here, $\hat{\beta}$ and β_{-1} are the cruise control gain and the backward-looking gain of the automated vehicle, respectively; while $W(v) = \min(v, v_{\max})$ is the velocity saturation function. Furthermore, we assume that the human driver is responding to the HV's relative velocity with respect to the AV with a control gain β, and also considers the so-called range policy $V(h_{-1})$ with the control gain α. Note that the saturation function $W(v)$ is non-smooth, which is a coarse approximation of human behavior, but this breakpoint is not reached in our domain of interest.

Figure 1(b) presents the nonlinear range policy function that determines the relation between the distance headway h and the corresponding desired velocity. We assume that if h gets smaller than the critical value h_{stop}, then the human driver intends to stop; while if the vehicle ahead is sufficiently far away, that is, $h > h_{\mathrm{go}}$, then the driver aims to travel with a comfortable $v_{\max}$ velocity. Finally, if the headway takes a value in between h_{stop} and h_{go}, then the driver is responding according to a strictly monotonically increasing function $F(h)$. Thus, the range policy function assumes the form

$$V(h) = \begin{cases} 0, & \text{if } h < h_{\mathrm{stop}}, \\ F(h), & \text{if } h_{\mathrm{stop}} \le h < h_{\mathrm{go}}, \\ v_{\max}, & \text{if } h_{\mathrm{go}} \le h. \end{cases} \tag{4}$$

Here, we approximate $F(h)$ with the third-degree polynomial

$$F(h) = v_{\max} \frac{(3h_{\mathrm{go}} - h_{\mathrm{stop}} - 2h)(h - h_{\mathrm{stop}})^2}{(h_{\mathrm{go}} - h_{\mathrm{stop}})^3}, \tag{5}$$

which introduces the relevant nonlinearity into the system.

This model of the human driver is called optimal velocity model, which is widely used in the literature [9,12,17,25]; moreover, the typical numerical values of the human gains α and β have already been measured and estimated in [2].

3 Linear Analysis

First, let us investigate the linearized dynamics to provide a basis of comparison for nonlinear studies.

In case of constant reference velocity $v_{\text{ref}}(t) = \bar{v}_{\text{ref}} < v_{\max}$, the governing equations (1)-(3) yield the steady state motion $v^{\star}_{-1} = v^{\star} = \bar{v}_{\text{ref}}$, while the inverse of the range policy determines the distance between the two vehicles: $h^{\star}_{-1} = V^{-1}(\bar{v}_{\text{ref}})$. As Fig. 1(b) presents, the slope of the range policy at the steady state is denoted by $\kappa = V'(h^{\star}_{-1})$.

Let us introduce the time varying reference velocity $v_{\text{ref}}(t) = \bar{v}_{\text{ref}} + \tilde{v}_{\text{ref}}(t)$ and the shifted state vector $\mathbf{x} = [\tilde{h}_{-1}\ \tilde{v}_{-1}\ \tilde{v}]^{\mathrm{T}}$ with

$$\tilde{h}_{-1} = h_{-1} - h^{\star}_{-1}, \quad \tilde{v}_{-1} = v_{-1} - \bar{v}_{\text{ref}}, \quad \text{and} \quad \tilde{v} = v - \bar{v}_{\text{ref}}, \tag{6}$$

which leads to the linearized state space model

$$\dot{\mathbf{x}} = \mathbf{A}\mathbf{x} + \mathbf{B}\tilde{v}_{\text{ref}}, \tag{7}$$

$$y = \mathbf{C}\mathbf{x}. \tag{8}$$

Here, the velocity of the HV is selected as the output y, and the coefficient matrices assume the form

$$\mathbf{A} = \begin{bmatrix} 0 & -1 & 1 \\ \alpha\kappa & -(\alpha+\beta) & \beta \\ 0 & \beta_{-1} & -(\hat{\beta}+\beta_{-1}) \end{bmatrix}, \quad \mathbf{B} = \begin{bmatrix} 0 \\ 0 \\ \hat{\beta} \end{bmatrix}, \quad \mathbf{C} = \begin{bmatrix} 0\ 1\ 0 \end{bmatrix}. \tag{9}$$

The stability of the linearized system can be analysed in two ways. On one hand, the system is called plant stable if it is stable at constant reference velocity $v_{\text{ref}} = \bar{v}_{\text{ref}}$; on the other hand, the system is called string stable if the oscillations in the input $\tilde{v}_{\text{ref}}(t)$ do not lead to increased oscillations in the output y.

3.1 Plant Stability

The plant stability is determined by the roots of the characteristic function $D(s) = \det(s\mathbf{I} - \mathbf{A})$ which leads to the characteristic equation

$$s^3 + (\alpha + \beta + \hat{\beta} + \beta_{-1})s^2 + (\alpha\hat{\beta} + \alpha\beta_{-1} + \beta\hat{\beta} + \alpha\kappa)s + \alpha\kappa\hat{\beta} = 0. \tag{10}$$

The system is stable if and only if all the characteristic roots have negative real parts. Because of Rouche's theorem, the location of the roots is a continuous function of the control gains. Thus, varying the parameters, the system may loose its stability in two ways: either a root crosses the imaginary axis through the origin of the complex plane leading to static loss of stability (steady-state bifurcation); or a pair of complex conjugate roots crosses the imaginary axis with nonzero imaginary part, which leads to dynamic loss of stability (Hopf bifurcation).

Thus, the static stability boundary can be determined by substituting $s = 0$ into Eq. (10), which yields

$$\alpha\kappa\hat{\beta} = 0. \tag{11}$$

Similarly, the dynamic stability boundary can be calculated by substituting $s = \mathrm{j}\Omega$ into the characteristic equation, where Ω is the angular frequency, with

which the system starts oscillating when it loses stability. This leads to a complex equation, the real and imaginary parts of which have to be 0 at the same time. From the system of the corresponding two scalar algebraic equations, the critical control gains of the AV can be expressed as the function of Ω:

$$\beta_{-1}(\Omega) = -\frac{\Omega^4 + ((\alpha+\beta)^2 - 2\alpha\kappa)\Omega^2 + \alpha^2\kappa^2}{\beta\Omega^2 + \alpha^2\kappa}, \tag{12}$$

$$\hat{\beta}(\Omega) = \frac{\Omega^4 + \alpha(\alpha+\beta-\kappa)\Omega^2}{\beta\Omega^2 + \alpha^2\kappa}. \tag{13}$$

Figure 2 presents a stability chart in the plane of the AV control gains β_{-1} and $\hat{\beta}$, while the control gains of the human driver are fixed (see [2]). The static and dynamic stability boundaries are denoted by dashed and solid red lines, respectively; both the dark and the light gray regions are plant stable. This means that the cruise control gain $\hat{\beta}$ has to be positive, while the backward-looking gain β_{-1} may also be tuned to negative values.

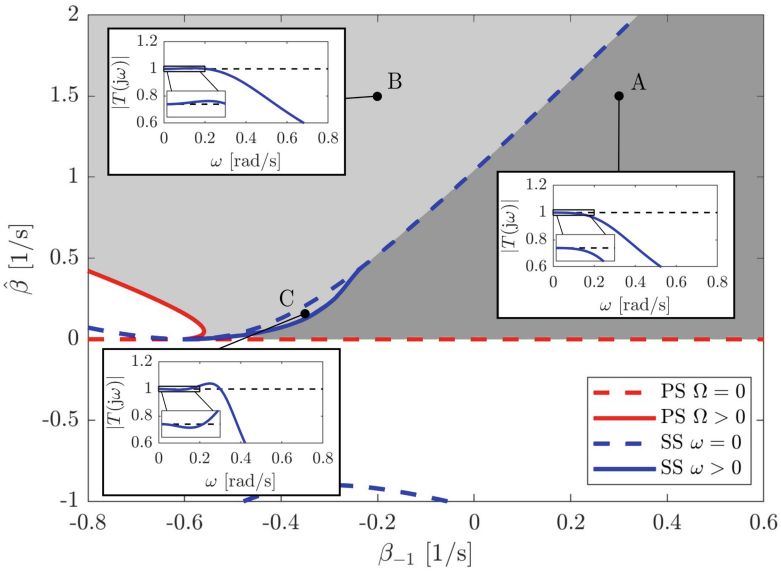

Fig. 2. Linear stability chart ($\alpha = 0.3\ \mathrm{s}^{-1}$, $\beta = 0.4\ \mathrm{s}^{-1}$, $\kappa = 0.6\ \mathrm{s}^{-1}$). Both the light gray and the dark gray regions are plant stable, while the dark gray region is also string stable. The inlets display typical frequency response curves at the corresponding control gain combinations.

3.2 String Stability

The string stability is defined by the transfer function between the input and the output of the system, which are now the reference velocity and the velocity

of the HV. The corresponding transfer function takes the form

$$T(s) = \mathbf{C}(s\mathbf{I} - \mathbf{A})^{-1}\mathbf{B} =: \frac{N(s)}{D(s)}, \tag{14}$$

where $D(s)$ is the same characteristic function as it was used in the plant stability calculations, while the numerator assumes the form

$$N(s) = s\beta\hat{\beta} + \alpha\kappa\hat{\beta}. \tag{15}$$

The system is called string stable if

$$|T(\mathrm{j}\omega)| < 1, \text{ for all } \omega > 0. \tag{16}$$

Again, two types of string instability may occur: in case of the string instability at $\omega = 0$, the norm of the transfer function goes above 1 immediately after $\omega = 0$; while in case of the string instability at an $\omega > 0$, the norm of the transfer function first decreases but it has a peak later, at which it exceeds 1.

As it is derived in [27], the $\omega = 0$ string instability boundary is located at

$$\hat{\beta} = -\beta_{-1}\frac{\alpha + \beta - \kappa}{\alpha + 2\beta - 2\kappa} \pm \frac{\sqrt{\beta_{-1}^2(\alpha + \beta - \kappa)^2 - \alpha(\alpha + 2\beta - 2\kappa)(\beta_{-1} + \kappa)^2}}{\alpha + 2\beta - 2\kappa}. \tag{17}$$

The closed-form expression of the $\omega > 0$ string instability boundary has a lengthy expression that is not manageable in the present format here.

In Fig. 2, the dashed and solid blue curves correspond to the $\omega = 0$ and to the $\omega > 0$ string stability boundaries, respectively. Therefore, the dark gray region is both plant and string stable. Furthermore, the inlets present some typical transfer functions at three different control gain configurations. At point A, the system is string stable and (16) is satisfied. At point B, the norm of the transfer function goes beyond 1 immediately after $\omega = 0$. Finally, point C is close to an $\omega > 0$ string stability boundary, that is, $|T(\mathrm{j}\omega)|$ first decreases then it exceeds 1 later, as shown in the inlet.

4 Effect of Nonlinearities

Taking into account the relevant nonlinearities of the range policy modifies both the plant dynamics and the string stability. Assuming constant reference velocities, stable or unstable self-excited oscillations will occur close to the dynamic stability boundaries, which originate from super- or subcritical Hopf bifurcations. Considering the nonlinear string stability, the corresponding nonlinear frequency response function (FRF) is a function of the perturbation amplitude and includes not only the basic harmonics but also higher ones. Moreover, in the case of asymmetric nonlinearites, it also contains a shift term. The actual paper focuses on the string stability and the corresponding nonlinear FRFs of the car following model.

Let us assume that the reference velocity is subjected to a sinusoidal perturbation $\tilde{v}_{\mathrm{ref}}(t) = \varepsilon \cos(\omega t)$ leading to $v_{\mathrm{ref}}(t) = \bar{v}_{\mathrm{ref}} + \varepsilon \cos(\omega t)$. In this case, the equation of motion will take the form of the nonlinear non-autonomous differential equation

$$\dot{\mathbf{x}} = \mathbf{A}\mathbf{x} + \mathbf{g}(\mathbf{x}) + \mathbf{B}\varepsilon \cos(\omega t), \tag{18}$$

where $\mathbf{g} = \mathbf{g}_2 + \mathbf{g}_3$ contains the second- and third-degree nonlinearities, respectively, which now assume the form

$$\mathbf{g}_2(\boldsymbol{\Phi}, \boldsymbol{\Psi}) = \begin{bmatrix} 0 \\ \frac{\alpha}{2} V''(h^\star_{-1}) \Phi_1 \Psi_1 \\ 0 \end{bmatrix}, \quad \mathbf{g}_3(\boldsymbol{\Phi}, \boldsymbol{\Psi}, \boldsymbol{\Lambda}) = \begin{bmatrix} 0 \\ \frac{\alpha}{6} V'''(h^\star_{-1}) \Phi_1 \Psi_1 \Lambda_1 \\ 0 \end{bmatrix}. \tag{19}$$

Subscript 1 denotes the first element of the 3-dimensional vectors $\boldsymbol{\Phi}$, $\boldsymbol{\Psi}$, or $\boldsymbol{\Lambda}$.

The nonlinear equation of motion (18) can not be solved in closed form, however, there are various approaches to approximate the solution analytically. In this paper, we apply the harmonic balance method [4,14,16].

4.1 Harmonic Balance

Since it is easier to work with exponential functions, let us substitute $\cos(\omega t)$ with the Euler's formula in (18):

$$\dot{\mathbf{x}} = \mathbf{A}\mathbf{x} + \mathbf{g}(\mathbf{x}) + \frac{1}{2}\mathbf{B}\varepsilon \left(\mathrm{e}^{\mathrm{j}\omega t} + \mathrm{e}^{-\mathrm{j}\omega t}\right). \tag{20}$$

In what follows, assume that the linear unexcited system is stable. In the case of small excitation amplitudes, it can be assumed that the $\mathcal{O}(\varepsilon)$ terms of the solution do not depend on the nonlinearities, that is, these form the solution of the excited linearized system. So, the solution is approximated as

$$\mathbf{x}(t) = \varepsilon \left(\mathbf{a}_{10}\mathrm{e}^{\mathrm{j}\omega t} + \mathbf{a}_{01}\mathrm{e}^{-\mathrm{j}\omega t}\right) + \mathcal{O}(\varepsilon^2). \tag{21}$$

Substituting (21) into the equation of motion (20), the coefficients of $\varepsilon \mathrm{e}^{\mathrm{j}\omega t}$ can be balanced:

$$\mathrm{j}\omega \mathbf{a}_{10} = \mathbf{A}\mathbf{a}_{10} + \frac{1}{2}\mathbf{B}, \tag{22}$$

which results in the solution

$$\mathbf{a}_{10} = \frac{1}{2}\left(\mathrm{j}\omega \mathbf{I} - \mathbf{A}\right)^{-1}\mathbf{B}. \tag{23}$$

Looking for the coefficients of $\varepsilon \mathrm{e}^{-\mathrm{j}\omega t}$ yields that $\mathbf{a}_{01} = \bar{\mathbf{a}}_{10}$, where overbar denotes the complex conjugate. This is consistent with the requirement that the solution $x(t)$ has to be a real function of time. The higher-order terms can be calculated successively by substituting the actual approximation of $x(t)$ in the

nonlinear equation of motion (20). The second- and third-order nonlinearities yield that the particular solution assumes the form

$$\begin{aligned}\mathbf{x}(t) = &\varepsilon\left(\mathbf{a}_{10}\mathrm{e}^{\mathrm{j}\omega t} + \mathbf{a}_{01}\mathrm{e}^{-\mathrm{j}\omega t}\right) + \varepsilon^2\left(\mathbf{a}_{20}\mathrm{e}^{2\mathrm{j}\omega t} + \mathbf{a}_{11} + \mathbf{a}_{02}\mathrm{e}^{-2\mathrm{j}\omega t}\right)\\ &+ \varepsilon^3\left(\mathbf{a}_{30}\mathrm{e}^{3\mathrm{j}\omega t} + \mathbf{a}_{21}\mathrm{e}^{\mathrm{j}\omega t} + \mathbf{a}_{12}\mathrm{e}^{-\mathrm{j}\omega t} + \mathbf{a}_{03}\mathrm{e}^{-3\mathrm{j}\omega t}\right) + \ldots.\end{aligned} \tag{24}$$

Note, that $\mathrm{e}^{j\omega t}$ terms appear not only in the coefficients of ε, but also in the coefficients of ε^3 and all higher-order terms with odd order. Thus, applying the harmonic balance method, the coefficients of $\varepsilon^2\mathrm{e}^{2\mathrm{j}\omega t}$ yield that

$$\mathbf{a}_{20} = \left(2\mathrm{j}\omega\mathbf{I} - \mathbf{A}\right)^{-1}\mathbf{g}_2(\mathbf{a}_{10}, \mathbf{a}_{10}), \tag{25}$$

while, again, $\mathbf{a}_{02} = \bar{\mathbf{a}}_{20}$.

As it can be expected from the presence of the second-degree nonlinearities, there will be a shift in the solution. This corresponds to the $\varepsilon^2\mathrm{e}^0$ terms, which yields

$$\mathbf{a}_{11} = -2\mathbf{A}^{-1}\mathbf{g}_2(\mathbf{a}_{10}, \mathbf{a}_{01}). \tag{26}$$

One can also calculate the $\mathbf{a}_{30}$ and $\mathbf{a}_{21}$ vectors from the balance of the coefficients of $\varepsilon^3\mathrm{e}^{3\mathrm{j}\omega t}$ and $\varepsilon^3\mathrm{e}^{\mathrm{j}\omega t}$. These take the form

$$\mathbf{a}_{30} = \left(3\mathrm{j}\omega\mathbf{I} - \mathbf{A}\right)^{-1}\left(2\mathbf{g}_2(\mathbf{a}_{10}, \mathbf{a}_{20}) + \mathbf{g}_3(\mathbf{a}_{10}, \mathbf{a}_{10}, \mathbf{a}_{10})\right), \tag{27}$$

$$\mathbf{a}_{21} = \left(\mathrm{j}\omega\mathbf{I} - \mathbf{A}\right)^{-1}\left(2\mathbf{g}_2(\mathbf{a}_{01}, \mathbf{a}_{20}) + 2\mathbf{g}_2(\mathbf{a}_{10}, \mathbf{a}_{11}) + 3\mathbf{g}_3(\mathbf{a}_{10}, \mathbf{a}_{10}, \mathbf{a}_{01})\right); \tag{28}$$

and finally, $\mathbf{a}_{03} = \bar{\mathbf{a}}_{30}$ and $\mathbf{a}_{12} = \bar{\mathbf{a}}_{21}$.

Note that neglecting the nonlinearity, the response will only be determined by $\mathbf{a}_{10} = \bar{\mathbf{a}}_{01}$; so, Eq. (23) together with Eq. (8) yield the transfer function (14).

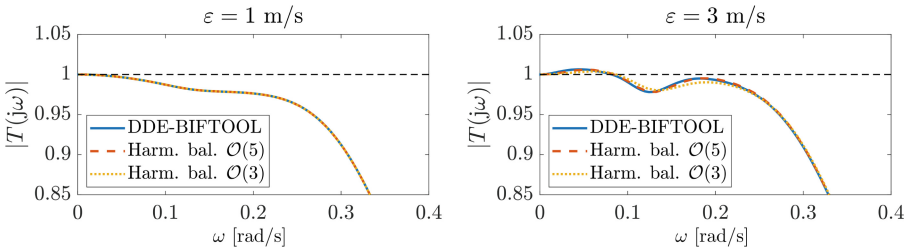

Fig. 3. Comparison of the nonlinear frequency response $M(\omega)$ calculated with 3rd and 5th order harmonic balance method and with the DDE-BIFTOOL package for excitation amplitudes $\varepsilon = 1$ m/s and $\varepsilon = 3$ m/s ($\alpha = 0.3$ s^{-1}, $\beta = 0.4$ s^{-1}, $\beta_{-1} = -0.3$ s^{-1}, $\hat{\beta} = 0.18$ s^{-1}, $v_{\max} = 30$ m/s, $\bar{v}_{\mathrm{ref}} = 26.55$ m/s, $h_{\mathrm{stop}} = 5$ m, $h_{\mathrm{go}} = 55$ m).

Let $M(\omega)$ denote the nonlinear magnification between the amplitude of oscillation of the reference velocity and that of the HV. Figure 3 compares this nonlinear magnification calculated with harmonic balance method up to 3rd and 5th order with the results of the DDE-BIFTOOL package in MATLAB [8] (see

details in the Appendix). As it can be observed, the frequency response depends on the amplitude of the excitation. If $\varepsilon = 1$ m/s, then the three curves run exactly on each other and the response is string stable; while in case of $\varepsilon = 3$ m/s, there is a slight difference between the responses. In this case, the 5^{th} order harmonic balance method approximates the continuation-based solution better, but all the three results show string unstable property. This comparison demonstrates the accuracy of the harmonic balance method, which is computationally more efficient than the continuation based solvers, making it a good candidate for performing multi-dimensional parameter analysis.

Figure 4 presents stability charts in the plane of the control gains of the AV, which are colored according to the maximum of the norm of the nonlinear frequency response. The linear string stability limit is recovered for small excitation amplitudes (cf. Fig. 2), while the string stable domain shrinks for small and extends for large values of $\hat{\beta}$, respectively, as the excitation amplitude is increased. Note, that the large values of $\hat{\beta}$ might lead to unrealistic large accelerations of the AV. Panel (c) of Fig. 4 shows the change of the transfer functions for the gains $\beta_{-1} = -0.3\ \text{s}^{-1}$ and $\hat{\beta} = 0.18\ \text{s}^{-1}$ as the excitation amplitude increases; this specific case was analysed in Fig. 3. Here, it can be observed in more detail how the nonlinear system loses its string stability as the excitation amplitude increases. Note that these figures are created using the 5^{th} order harmonic balance method, which still does not take into account either the saturation of the range policy function or the velocity saturation $W(v)$. However, in case of the string stable and the slightly string unstable solutions, these saturation scenarios do not occur.

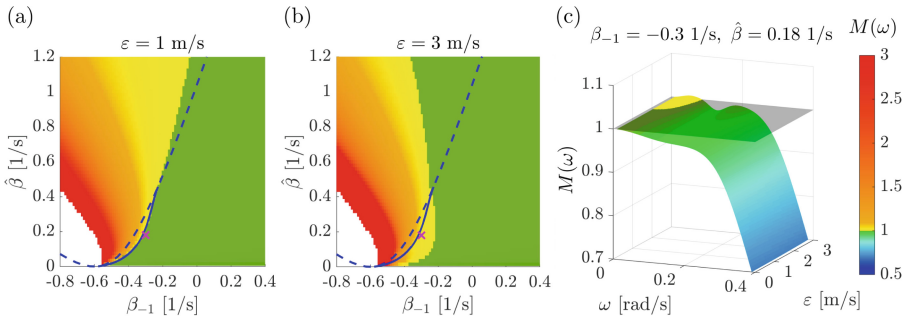

Fig. 4. Panels (a) and (b) present stability charts in case of different excitation amplitudes colored according to the maximum of the norm of the frequency response function ($\alpha = 0.3\ \text{s}^{-1}$, $\beta = 0.4\ \text{s}^{-1}$, $v_{\max} = 30$ m/s, $\bar{v}_{\text{ref}} = 26.55$ m/s, $h_{\text{stop}} = 5$ m, $h_{\text{go}} = 55$ m). The green region is plant and string stable, while the blue dashed and continuous lines refer to linear string stability boundaries. Panel (c) shows the change of the frequency response curves as the excitation amplitude increases (for the parameter combination $\beta_{-1} = -0.3\ \text{s}^{-1}$, $\hat{\beta} = 0.18\ \text{s}^{-1}$, marked with magenta crosses in the stability charts).

5 Conclusion

In this study, we investigated the dynamics of an HV following an AV equipped with a backward-looking control. The results of the linear analysis showed that it is advisable to apply small positive values for the cruise control gain, while the backward-looking gain can take both positive and negative values. However, taking into account the nonlinearities in the range policy function, we found that the backward looking gain should be increased. Measurements are to be performed in the future to tune the model of the human driver and verify the theoretical results. This will enable us to design control systems for automated vehicles and guide the dynamics of the traffic flow in mixed traffic scenarios.

Appendix

The DDEBIFTOOL MATLAB package is a continuation based solver primarily developed for the analysis of delay differential equations but it can also work with autonomous systems without delay [8]. Although, our system is non-autonomous, it can be transformed to an autonomous ODE by extending it with a two dimensional subsystem, the periodic solution of which is $[y(t),\ z(t)]^{\mathrm{T}} = [\sin(\omega t + \gamma),\ \cos(\omega t + \gamma)]^{\mathrm{T}}$. The extended ODE takes the form

$$\begin{bmatrix} \dot{\mathbf{x}} \\ \dot{y} \\ \dot{z} \end{bmatrix} = \begin{bmatrix} \mathbf{A} & \mathbf{0} & \varepsilon\mathbf{B} \\ \mathbf{0} & 1 & \omega \\ \mathbf{0} & -\omega & 1 \end{bmatrix} \begin{bmatrix} \mathbf{x} \\ y \\ z \end{bmatrix} + \begin{bmatrix} \mathbf{g}(\mathbf{x}) \\ -y(y^2+z^2) \\ -z(y^2+z^2) \end{bmatrix}, \tag{29}$$

the periodic solution of which is the same as that of the original system (18).

References

1. Ahmadi, H., Foroutan, K.: Nonlinear primary resonance of spiral stiffened functionally graded cylindrical shells with damping force using the method of multiple scales. Thin-Walled Struct. **135**, 33–44 (2019)
2. Avedisov, S.S., Bansal, G., Orosz, G.: Impacts of connected automated vehicles on freeway traffic patterns at different penetration levels. IEEE Trans. Intell. Transp. Syst. **23**(5), 4305–4318 (2022)
3. Besselink, B., Johansson, K.H.: String stability and a delay-based spacing policy for vehicle platoons subject to disturbances. IEEE Trans. Autom. Control **62**(9), 4376–4391 (2017)
4. Blahoš, J., Vizzaccaro, A., Salles, L., El Haddad, F.: Parallel harmonic balance method for analysis of nonlinear dynamical systems. In: Turbo Expo: Power for Land, Sea, and Air, vol. 84232. American Society of Mechanical Engineers (2020). V011T30A028
5. Breunung, T., Haller, G.: Explicit backbone curves from spectral submanifolds of forced-damped nonlinear mechanical systems. Proc. Roy. Soc. A: Math. Phys. Eng. Sci. **474**(2213), 20180083 (2018)
6. Caveney, D.: Cooperative vehicular safety applications. IEEE Control Syst. Mag. **30**(4), 38–53 (2010)

7. Chan, E., Gilhead, P., Jelinek, P., Krejci, P., Robinson, T.: Cooperative control of SARTRE automated platoon vehicles. In: Proceedings of the 19th ITS World Congress, Vienna (2012)
8. Engelborghs, K., Luzyanina, T., Samaey, G., et al.: DDE-BIFTOOL: a Matlab package for bifurcation analysis of delay differential equations. TW Report **305**(1) (2000)
9. Gisolo, C.M., Delle Monache, M.L., Ferrante, F., Frasca, P.: Nonlinear analysis of stability and safety of optimal velocity model vehicle groups on ring roads. IEEE Trans. Intell. Transp. Syst. **23**(11), 20628–20635 (2022)
10. Guo, S., Orosz, G., Molnar, T.G.: Connected cruise and traffic control for pairs of connected automated vehicles. IEEE Trans. Intell. Transp. Syst. **24**(11), 12648–12658 (2023)
11. Haller, G., Ponsioen, S.: Nonlinear normal modes and spectral submanifolds: existence, uniqueness and use in model reduction. Nonl. Dyn. **86**, 1493–1534 (2016)
12. Jin, Y., Meng, J.: Dynamical analysis of an optimal velocity model with time delayed feedback control. Commun. Nonl. Sci. Numer. Simulat. **90**, 105333 (2020)
13. Jones, J.P., Yaser, K.: Computation of the MIMO Volterra frequency response functions of nonlinear systems. Mech. Syst. Signal Process. **134**, 106323 (2019)
14. Krack, M., Gross, J.: Harmonic Balance for Nonlinear Vibration Problems, vol. 1. Springer (2019)
15. Lelkes, J., Kalmár-Nagy, T.: Bifurcation analysis of a forced delay equation for machine tool vibrations. Nonl. Dyn. **98**(4), 2961–2974 (2019). https://doi.org/10.1007/s11071-019-04984-w
16. Marathe, A., Chatterjee, A.: Wave attenuation in nonlinear periodic structures using harmonic balance and multiple scales. J. Sound Vib. **289**(4–5), 871–888 (2006)
17. Martinovich, K., Kiss, A.K.: Nonlinear effects of saturation in the car-following model. Nonl. Dyn. **111**(3), 2555–2569 (2023)
18. Molnár, T.G., Hopka, M., Upadhyay, D., Van Nieuwstadt, M., Orosz, G.: Virtual rings on highways: traffic control by connected automated vehicles. In: AI-enabled Technologies for Autonomous and Connected Vehicles, pp. 441–479. Springer (2023)
19. Nayfeh, A.H.: Resolving controversies in the application of the method of multiple scales and the generalized method of averaging. Nonl. Dyn. **40**, 61–102 (2005)
20. Orosz, G.: Connected cruise control: modelling, delay effects, and nonlinear behaviour. Veh. Syst. Dyn. **54**(8), 1147–1176 (2016)
21. Peng, Z., Lang, Z., Billings, S., Tomlinson, G.: Comparisons between harmonic balance and nonlinear output frequency response function in nonlinear system analysis. J. Sound Vib. **311**(1–2), 56–73 (2008)
22. Ploeg, J., van de Wouw, N., Nijmeijer, H.: L_p string stability of cascaded systems: application to vehicle platooning. IEEE Trans. Control Syst. Technol. **22**(2), 786–793 (2014)
23. Qin, W.B., Gomez, M.M., Orosz, G.: Stability and frequency response under stochastic communication delays with applications to connected cruise control design. IEEE Trans. Intell. Transp. Syst. **18**(2), 388–403 (2017)
24. Rugh, W.J.: Nonlinear System Theory. Johns Hopkins University Press, Baltimore (1981)
25. Shen, M., He, C.R., Molnar, T.G., Bell, A.H., Orosz, G.: Energy-efficient connected cruise control with lean penetration of connected vehicles. IEEE Trans. Intell. Transp. Syst. **24**(4), 4320–4332 (2023)

26. Swaroop, D., Hedrick, J.K.: String stability of interconnected systems. IEEE Trans. Autom. Control **41**(3), 349–357 (1996)
27. Szaksz, B., Orosz, G., Stepan, G.: Guided control of a human driver via an automated vehicle. IFAC-PapersOnLine **56**(2), 899–904 (2023)
28. Wang, J., Zheng, Y., Chen, C., Xu, Q., Li, K.: Leading cruise control in mixed traffic flow: System modeling, controllability, and string stability. IEEE Trans. Intell. Transp. Syst. (2021)
29. Zhang, L., Orosz, G.: Motif-based design for connected vehicle systems in presence of heterogeneous connectivity structures and time delays. IEEE Trans. Intell. Transp. Syst. **17**(6), 1638–1651 (2016)